Enhanced visualization of peripheral retinal vasculature with wavefront sensorless adaptive optics OCT angiography in diabetic patients

James Polans[1,*], **David Cunefare**[1], **Eli Cole**[1], **Brenton Keller**[1], **Priyatham S. Mettu**[2], **Scott W. Cousins**[2], **Michael J. Allingham**[2], **Joseph A. Izatt**[1,2], and **Sina Farsiu**[1,2]

[1]Department of Biomedical Engineering, Duke University, 136 Hudson Hall, Box 90281, Durham, North Carolina 27708, USA

[2]Department of Ophthalmology, Duke University Medical Center, Durham, North Carolina 27710, USA

Abstract

Optical coherence tomography angiography (OCTA) is a promising technique for non-invasive visualization of vessel networks in the human eye. We debut a system capable of acquiring wide field-of-view (>70°) OCT angiograms without mosaicking. Additionally, we report on enhancing the visualization of peripheral microvasculature using wavefront sensorless adaptive optics (WSAO). We employed a fast WSAO algorithm that enabled wavefront correction in <2 seconds by iterating the mirror shape at the speed of OCT B-scans rather than volumes. Also, we contrasted ~7° field-of-view OCTA angiograms acquired in the periphery with and without WSAO correction. On average, WSAO improved the sharpness of microvasculature by 65% in healthy and 38% in diseased eyes. Preliminary observations demonstrated that the location of 7° images could be identified directly from the wide field-of-view angiogram. A pilot study on a normal subject and patients with diabetic retinopathy showed the impact of utilizing WSAO for OCTA when visualizing peripheral vasculature pathologies.

Similar to fluorescein angiography and indocyanine green video angiography, optical coherence tomography angiography (OCTA) [1–3] can visualize vessel networks in the human eye. OCTA offers an appealing alternative to dye-based angiography because rather than using a intraveinous fluorescent dye that may cause side effects ranging from nausea to allergic reactions [4], OCTA uses signal intensity fluctuations as an intrinsic contrast metric to distinguish blood flow from static tissue [5]. As pathologic changes in ocular vasculature, such as alterations in blood flow, vascular perfusion, vessel diameter, and growth of aberrant neovascular tissue, are associated with diverse ocular diseases including glaucoma, diabetic retinopathy, age-related macular degeneration, and retinitis pigmentosa [4, 6], OCTA has become an increasingly important tool for diagnosing diseases of the retina.

*Corresponding author: james.polans@duke.edu.

Despite the recent popularity of OCTA for analyzing parafoveal microvasculature, utilization of OCTA for diagnosing diseases affecting the peripheral retina [7], such as diabetic retinopathy and retinal vein occlusion, has been hindered by its limited field-of-view (FOV) and relatively slow acquisition time (as compared to structural OCT imaging). The rapid motion of microsaccades often leaves OCTA scans with blocks of missing data. In order to correct these artifacts, additional scans with tracking [8, 9] or redundancy have been acquired and then registered to fill in missing information [10] or to create a larger, mosaicked FOV [11, 12].

Even after motion correction, retinal OCT image quality is not consistent across a wide FOV [13] due to varying dynamic and static wavefront aberrations [14, 15]. An option to address this problem is adaptive optics with closed-loop feedback, wherein a wavefront sensor detects and a deformable mirror compensates optical aberrations [16, 17]. However, closed-loop adaptive optics with a wavefront sensor has a limited FOV and a large physical footprint. Additionally, off-axis wavefront detection, which is used in wide-field imaging, is vulnerable to errors in wavefront detection, a problem accentuated in peripheral regions of diseased eyes where the wavefront signal is weak.

In this work, we show that OCTA imaging of peripheral vasculature in normal and diseased retina is negatively impacted if aberrations are not corrected, and we demonstrate a compact OCTA system integrated with wavefront sensorless adaptive optics (WSAO) [18, 19] technology in order to overcome the loss of peripheral image quality. WSAO uses image quality metrics, such as brightness, to correct the wavefront iteratively using a deformable mirror. Using image quality metrics to correct the wavefront allows WSAO to be less sensitive to cataracts or elliptically shaped pupils, which is relevant especially when imaging peripheral pathologies. Our fast WSAO algorithm enabled peripheral wavefront correction in <2 s by iterating the mirror shape at the speed of OCT B-scans rather than iterating by OCT volumes. We demonstrated that equipping wide-field (>70° external beam angle) optical coherence tomography (WF-OCT) with WSAO enhanced the visualization of targeted OCT angiograms in the retinal periphery. We acquired wide FOV (~70°) OCT angiograms without mosaicking, and we contrasted ~7° patches of peripheral microvasculature obtained with and without WSAO correction. The wide FOV angiogram was helpful in identifying the location of peripheral WSAO-enhanced microvascular images. A pilot study consisting of a normal subject and three patients with diabetic retinopathy revealed that WSAO enabled the visualization of peripheral microaneurysms.

Recently, we described our WSAO enabled WF-OCT hardware in detail and demonstrated its utility in structural imaging applications [20]. In summary, our system was based on a 1043 nm, 100 nm bandwidth, 100 kHz swept-source OCT engine with a peak sensitivity of 103 dB with an axial resolution of 7.24 μm and a −6 dB sensitivity fall-off at 5.24 mm. The sample arm was capable of achieving a FOV of 70° without vignetting a 3 mm diameter beam incident on the cornea and included a deformable mirror (Mirao-52e, Imagine Optic, Inc.; Boston, MA) conjugate with the pupil of the subject's eye. Pupil dilation (>6 mm) was accomplished by darkening the room. The footprint of the sample arm of our compact system was approximately 400 mm by 600 mm. Adaptive optics OCT correction of low-order aberrations with a 3 mm beam was originally pioneered in [21].

A host of different WSAO optimization algorithms have been studied previously, but only a handful have been used specifically for ophthalmic OCT, including coordinate search using Zernike modes [19, 22] and stochastic parallel gradient descent [18]. The best ophthalmic WSAO-OCT imaging systems have demonstrated convergence times on the order of 10 s in human eyes [23]. Our algorithm typically converged within 100–150 iterations (1.2–1.8 s) in the human eye which was as fast as more computationally complex algorithms that have been used on static targets [24]. Our WSAO optimization algorithm was based on the coordinate search method of [19], which applied Zernike terms (Z3–Z9) sequentially to the mirror and selected coefficients that produced the largest optimization metric. The method used in this manuscript differs from that of [19] in that our technique used the spectral interferogram from unprocessed OCT B-scans to calculate the optimization metric. Additionally, the algorithm varied in that it first stepped coarsely ($1/10^{th}$ of the mirror's dynamic range) through each Zernike term and then searched with finer ($1/100^{th}$) steps around the best recorded value. For each Zernike term, the fine sweep centered its search range on the best coefficient value from the prior sweep, which allowed the algorithm to converge even if the eye moved from the start of the optimization process. The order of optimization was defocus, horizontal astigmatism, vertical astigmatism, vertical trefoil, vertical coma, horizontal coma, oblique trefoil, spherical aberration.

Three types of images were acquired in the volunteers:

1. wide-field (up to 70° or 22×22 mm) OCTA without WSAO correction

2. targeted OCTA from a peripheral region (~7° or 2×2 mm) without WSAO correction

3. targeted OCTA from a peripheral region (~7° or 2×2 mm) with WSAO correction

A total of four subjects (one healthy control and three volunteers with diabetic retinopathy) were imaged. All subjects were imaged in accordance with an approved Duke University Institutional Review Board protocol.

To provide an overview of vascular structure, wide-field OCTA volumes with three repeated B-scans were acquired. This provided a single OCTA volume consisting of 600 samples in the front sweep, 600 samples in the back sweep, 1800 samples in the transverse direction, and 1280 samples in the axial direction. No WSAO correction was applied to the wide-field images.

Targeted (less than 2×2 mm) high-resolution peripheral images consisting of three repeated B-scan volumes with the fast scan axis in the × (Xfast) or y (Yfast) direction [10] were acquired both with and without WSAO wavefront correction. A new wavefront shape was determined immediately prior to each WSAO optimized image. These scan protocols were comprised of 300 samples in the front sweep, 292 samples in the back sweep, 900 samples in the transverse direction, and 1280 samples in the axial direction. In summary, for each targeted peripheral retinal location, four volumes (WSAO off Xfast, WSAO off Yfast, WSAO on Xfast, WSAO on Yfast) were acquired, each containing an image from its front and back sweep.

OCTA angiograms for both targeted image patches as well as wide-field angiograms were processed according to the following protocol. Raw spectral OCT data was DC subtracted and numerical dispersion compensated prior to FFT and log transforms. Repeated B-scans (three throughout this paper) were averaged and the outlying 2% of the histogram intensity data were truncated. The resulting images were semi-automatically segmented using DOCTRAP software [25]. Two variance images were produced: one from each of the front and back galvanometer sweeps. The two variance images were registered and rescaled to each other using cross-correlation and then averaged. This process was applied to both Xfast and Yfast volumes. Xfast and Yfast volumes were registered together using a strip-based method [11]. Image sharpness was calculated using the method outlined in [26] with a spatial frequency cut-off of $1/105 \ \mu m^{-1}$. **Error! Reference source not found.**(b) was displayed with the same contrast throughout the volume and depicts accurately the change in brightness with WSAO correction. The images in Figs. 2, 3, 4 were contrast adjusted in order to fairly compare vasculature without bias to image brightness.

While the fine sweep could loop indefinitely, we stopped the optimization after it reached a steady-state value, which was typically less than 2 s. It took 6 ms to acquire B-scan data, 1 ms to calculate the intensity metric, and 5 ms to update the deformable mirror. This allowed for a new mirror shape to be applied every 12 ms, as the optimization metric was calculated after the mirror settled for a full B-scan [20].

A sample wide-field OCT angiogram in a normal subject (**Error! Reference source not found.**(a)) highlights the region in which OCTA was performed without changing subject fixation. Though WSAO can be applied throughout this entire FOV over smaller patches, no correction was applied for the wide-field image in **Error! Reference source not found.**(a), as this FOV greatly exceeded the isoplanatic patch. This single (unaveraged) image was taken in a healthy volunteer in a single continuous acquisition that lasted 21.6 s.

Error! Reference source not found.(b) shows a continuous volume scan in which midway through the volume scan the deformable mirror was changed from a WSAO optimized mirror shape (top) to a flat mirror shape (bottom). This figure illustrates both a change in signal intensity as well as a change in the visibility of features for co-localized regions. The yellow box in **Error! Reference source not found.**(a) corresponds to the location of **Error! Reference source not found.**(b).

Fig. 2 contrasts the effect of WSAO correction in a series of images taken in the periphery of a healthy human eye. The data of Fig. 2 was obtained from the peripheral region bounded by the red box in **Error! Reference source not found.**(a). The left-half of image pairs represent images taken without WSAO correction, and the right-half with WSAO correction. The pairs of OCTA images were registered to each other after correcting motion artifacts [11]. In each of the image pairs the image contrast improved with WSAO correction, resulting in better visualization of both the microvasculature and larger upper retinal vessels. It was difficult to discern the connectivity of the smaller microvasculature in many of the uncorrected (left-half) images. WSAO correction improved the image sharpness in Fig. 2's top, middle, and bottom image pairs by 45%, 53%, and 97%. The black background patches represent regions of the images that could not be recovered due to motion.

A similar series of peripheral images was compiled for the volunteers with diabetic retinopathy (Fig. 3). All three subjects had cataracts, but only diabetic subjects 1 and 3 had cataract extraction. Again the vessel boundaries were better defined when WSAO correction was applied, but additionally, the sites of microaneurysms (yellow arrows) were also better visualized. While a number of microaneurysms were present in the images, it was interesting to note in the uncorrected images that the pathological sites could be mistaken for blurry vessel networks. It was much easier to distinguish microaneurysms when the wavefront was corrected. The image sharpness was enhanced 20%, 35%, and 60% by WSAO in Fig. 3's top, middle, and bottom image pairs. Note that the apparent double rendering of vasculature in the uncorrected images was not likely due to motion artifact, as this feature spanned the entire volume. Rather, it may have been caused by higher order aberrations such as astigmatism and coma that were corrected with WSAO.

Fig. 4 provides context for the amount of motion correction required in peripheral OCTA. While registered motion-corrected images are helpful for comparing images with and without WSAO correction, this requires a considerable amount of post-acquisition image processing. While a number of research groups are working to correct these artifacts [8–12, 27], it is easy to appreciate the benefits of WSAO even in the presence of motion.

Fig. 4 (left) shows a pair of images acquired at the boundary of the wide-field system's field-of-view (note the black boundary that defines the aperture of the system). Even at the peripheral extrema, the benefits of WSAO were clear as there was considerable microvasculature at this eccentricity. While microsaccades may have contributed to the sharpness values, the sharpness improved by 35%, 55%, and 12% in Fig. 4's left, middle, and right image pairs. WSAO may not have corrected the higher-order aberrations as well as closed-loop adaptive optics with a wavefront sensor, but the evidence provided in this Letter suggests that WSAO may improve OCTA sufficiently for the study of relatively small features in the peripheral retina, including microvasculature and microaneurysms.

Lastly, the wide-field angiogram (**Error! Reference source not found.**) was under sampled in order to keep the acquisition time around 20 s. While a 20 s acquisition time is not amenable to clinical practice, faster OCT engines are being developed each year [28]. However, it is important to keep in mind that even if the OCT A-line rate was faster, the wavefront correction would need to vary with retinal eccentricity [14]. While our WSAO enabled WF-OCT system can be used to mosaic wavefront corrected patches, we have found that imaging the entire retina at once and then targeting specific regions has worked well in our preliminary clinical encounters.

In summary, we have demonstrated the utility of WSAO when visualizing the microvasculature of the peripheral retina. OCTA was performed on a wide-field OCTA system within a 70° field-of-view and yielded quantifiable improvements in OCTA image sharpness. The WSAO technique used in this work was able to correct peripheral aberrations within 2 s to a level that was sufficient for the enhanced visualization of microvasculatures and microaneurysms in diabetic patients.

Acknowledgments

References

1. Yazdanfar S, Kulkarni MD, Izatt JA. High resolution imaging of in vivo cardiac dynamics using color Doppler optical coherence tomography. Opt Express. 1997; 1:424–431. [PubMed: 19377566]

2. Makita S, Hong Y, Yamanari M, Yatagai T, Yasuno Y. Optical coherence angiography. Opt Express. 2006; 14:7821–7840. [PubMed: 19529151]

3. Wang RK, Jacques SL, Ma Z, Hurst S, Hanson SR, Gruber A. Three dimensional optical angiography. Opt Express. 2007; 15:4083–4097. [PubMed: 19532651]

4. de Carlo TE, Romano A, Waheed NK, Duker JS. A review of optical coherence tomography angiography (OCTA). International Journal of Retina and Vitreous. 2015; 1:1–15. [PubMed: 27847594]

5. Mariampillai A, Standish BA, Moriyama EH, Khurana M, Munce NR, Leung MKK, Jiang J, Cable A, Wilson BC, Vitkin IA, Yang VXD. Speckle variance detection of microvasculature using swept-source optical coherence tomography. Opt Lett. 2008; 33:1530–1532. [PubMed: 18594688]

6. Zhang QQ, Lee CS, Chao J, Chen CL, Zhang T, Sharma U, Zhang AQ, Liu J, Rezaei K, Pepple KL, Munsen R, Kinyoun J, Johnstone M, Van Gelder RN, Wang RKK. Wide-field optical coherence tomography based microangiography for retinal imaging. Sci Rep-Uk. 2016; 6

7. Jia YL, Bailey ST, Hwang TS, McClintic SM, Gao SS, Pennesi ME, Flaxel CJ, Lauer AK, Wilson DJ, Hornegger J, Fujimoto JG, Huang D. Quantitative optical coherence tomography angiography of vascular abnormalities in the living human eye. P Natl Acad Sci USA. 2015; 112:E2395–E2402.

8. Braaf B, Vienola KV, Sheehy C, Yang Q, Vermeer KA, Tiruveedhula P, Arathorn DW, Roorda A, de Boer JF. Real-time eye motion correction in phase-resolved OCT angiography with tracking SLO. Biomed Opt Express. 2012; 4:51–65. [PubMed: 23304647]

9. Camino A, Zhang M, Gao SS, Hwang TS, Sharma U, Wilson DJ, Huang D, Jia Y. Evaluation of artifact reduction in optical coherence tomography angiography with real-time tracking and motion correction technology. Biomed Opt Express. 2016; 7:3905–3915. [PubMed: 27867702]

10. Kraus MF, Potsaid B, Mayer MA, Bock R, Baumann B, Liu JJ, Hornegger J, Fujimoto JG. Motion correction in optical coherence tomography volumes on a per A-scan basis using orthogonal scan patterns. Biomed Opt Express. 2012; 3:1182–1199. [PubMed: 22741067]

11. Hendargo HC, Estrada R, Chiu SJ, Tomasi C, Farsiu S, Izatt JA. Automated non-rigid registration and mosaicing for robust imaging of distinct retinal capillary beds using speckle variance optical coherence tomography. Biomed Opt Express. 2013; 4:803–821. [PubMed: 23761845]

12. Zang P, Liu G, Zhang M, Dongye C, Wang J, Pechauer AD, Hwang TS, Wilson DJ, Huang D, Li D, Jia Y. Automated motion correction using parallel-strip registration for wide-field en face OCT angiogram. Biomed Opt Express. 2016; 7:2823–2836. [PubMed: 27446709]

13. Kolb JP, Klein T, Kufner CL, Wieser W, Neubauer AS, Huber R. Ultra-widefield retinal MHz-OCT imaging with up to 100 degrees viewing angle. Biomed Opt Express. 2015; 6:1534–1552. [PubMed: 26137363]

14. Polans J, Jaeken B, McNabb RP, Artal P, Izatt JA. Wide-field optical model of the human eye with asymmetrically tilted and decentered lens that reproduces measured ocular aberrations. Optica. 2015; 2:124–134.

15. Jaeken B, Artal P. Optical Quality of Emmetropic and Myopic Eyes in the Periphery Measured with High-Angular Resolution. Invest Ophth Vis Sci. 2012; 53:3405–3413.

16. Zawadzki RJ, Jones SM, Olivier SS, Zhao MT, Bower BA, Izatt JA, Choi S, Laut S, Werner JS. Adaptive-optics optical coherence tomography for high-resolution and high-speed 3D retinal in vivo imaging. Opt Express. 2005; 13:8532–8546. [PubMed: 19096728]

17. Kocaoglu OP, Lee S, Jonnal RS, Wang Q, Herde AE, Derby JC, Gao W, Miller DT. Imaging cone photoreceptors in three dimensions and in time using ultrahigh resolution optical coherence tomography with adaptive optics. Biomed Opt Express. 2011; 2:748–763. [PubMed: 21483600]

18. Hofer H, Sredar N, Queener H, Li CH, Porter J. Wavefront sensorless adaptive optics ophthalmoscopy in the human eye. Opt Express. 2011; 19:14160–14171. [PubMed: 21934779]

19. Bonora S, Zawadzki RJ. Wavefront sensorless modal deformable mirror correction in adaptive optics: optical coherence tomography. Opt Lett. 2013; 38:4801–4804. [PubMed: 24322136]

20. Polans J, Keller B, Carrasco-Zevallos OM, LaRocca F, Cole E, Whitson HE, Lad EM, Farsiu S, Izatt JA. Wide-field retinal optical coherence tomography with wavefront sensorless adaptive optics for enhanced imaging of targeted regions. Biomed Opt Express. 2017; 8:16–37. [PubMed: 28101398]

21. Sudo K, Cense B. Adaptive optics-assisted optical coherence tomography for imaging of patients with age related macular degeneration. Ophthalmic Technologies. 2013; Xxiii:8567.

22. Jian YF, Xu J, Gradowski MA, Bonora S, Zawadzki RJ, Sarunic MV. Wavefront sensorless adaptive optics optical coherence tomography for in vivo retinal imaging in mice. Biomed Opt Express. 2014; 5:547–559. [PubMed: 24575347]

23. Wong KSK, Jian Y, Cua M, Bonora S, Zawadzki RJ, Sarunic MV. In vivo imaging of human photoreceptor mosaic with wavefront sensorless adaptive optics optical coherence tomography. Biomed Opt Express. 2015; 6:580–590. [PubMed: 25780747]

24. Verstraete HRGW, Wahls S, Kalkman J, Verhaegen M. Model-based sensor-less wavefront aberration correction in optical coherence tomography. Opt Lett. 2015; 40:5722–5725. [PubMed: 26670496]

25. Chiu SJ, Li XT, Nicholas P, Toth CA, Izatt JA, Farsiu S. Automatic segmentation of seven retinal layers in SDOCT images congruent with expert manual segmentation. Opt Express. 2010; 18:19413–19428. [PubMed: 20940837]

26. LaRocca F, Dhalla AH, Kelly MP, Farsiu S, Izatt JA. Optimization of confocal scanning laser ophthalmoscope design. J Biomed Opt. 2013; 18

27. Zhang QQ, Huang YP, Zhang T, Kubach S, An L, Laron M, Sharma U, Wang RKK. Wide-field imaging of retinal vasculature using optical coherence tomography-based microangiography provided by motion tracking. J Biomed Opt. 2015; 20

28. Klein T, Wieser W, Andre R, Pfeiffer T, Eigenwillig CM, Huber R. Multi-MHz FDML OCT: Snapshot retinal imaging at 6.7 million axial-scans per second. Optical Coherence Tomography and Coherence Domain Optical Methods in Biomedicine. 2012; Xvi:8213.
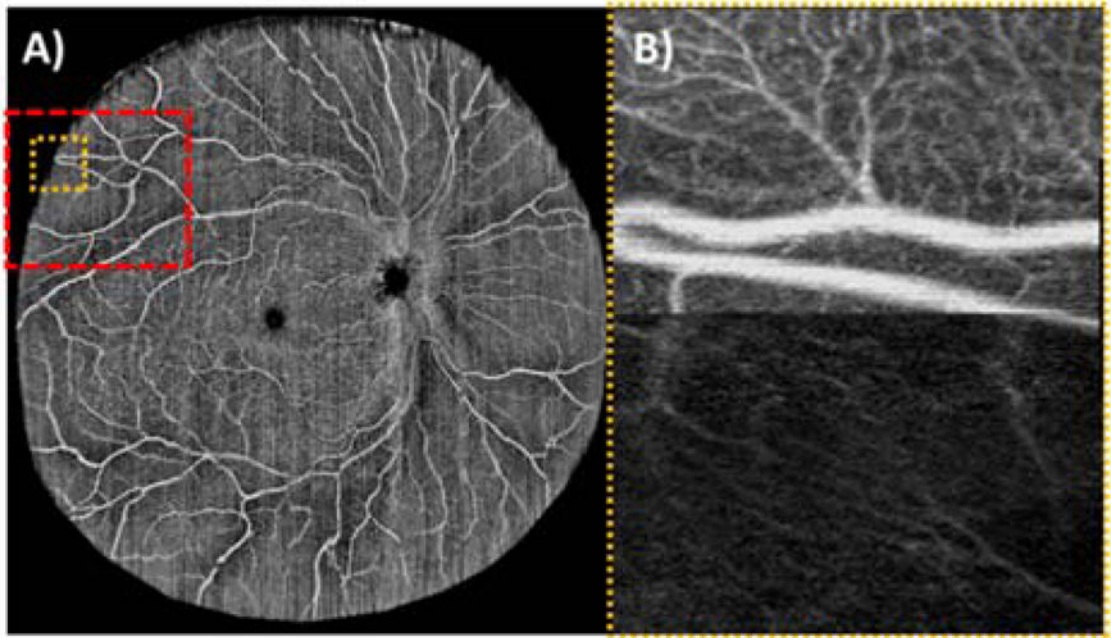
Fig. 1.
Single (unaveraged) wide-field (~65°) OCTA acquired in a healthy volunteer from a single continuous acquisition (left). The orange box corresponds to the location of a peripheral OCTA scan (right) in which the deformable mirror was toggled from an optimized (top) to flat (bottom) mirror shape. The toggled image is 1.45 (width) × 2.00 (height) mm. The red box corresponds to the regions in Fig. 2.
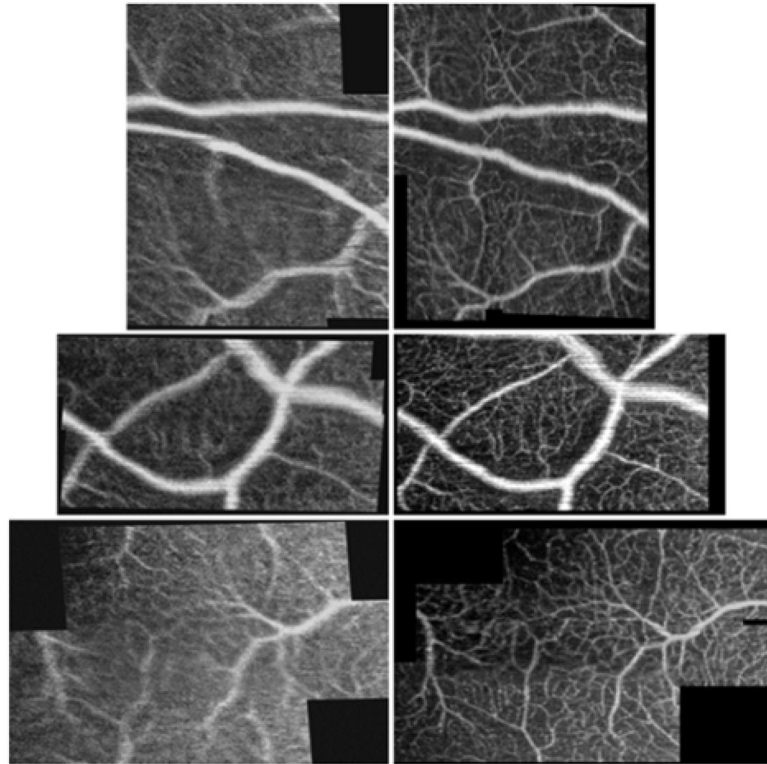
Fig. 2.
Targeted OCTA scans of peripheral microvasculature acquired without (left) and with (right) WSAO correction in a healthy volunteer. In all images, it was clear that the visibility of smaller vessels improved after WSAO correction. The images are 1.59×2.00 mm (top), 1.89×1.03 mm (middle), 2.17×1.39 mm (bottom) including the black space.
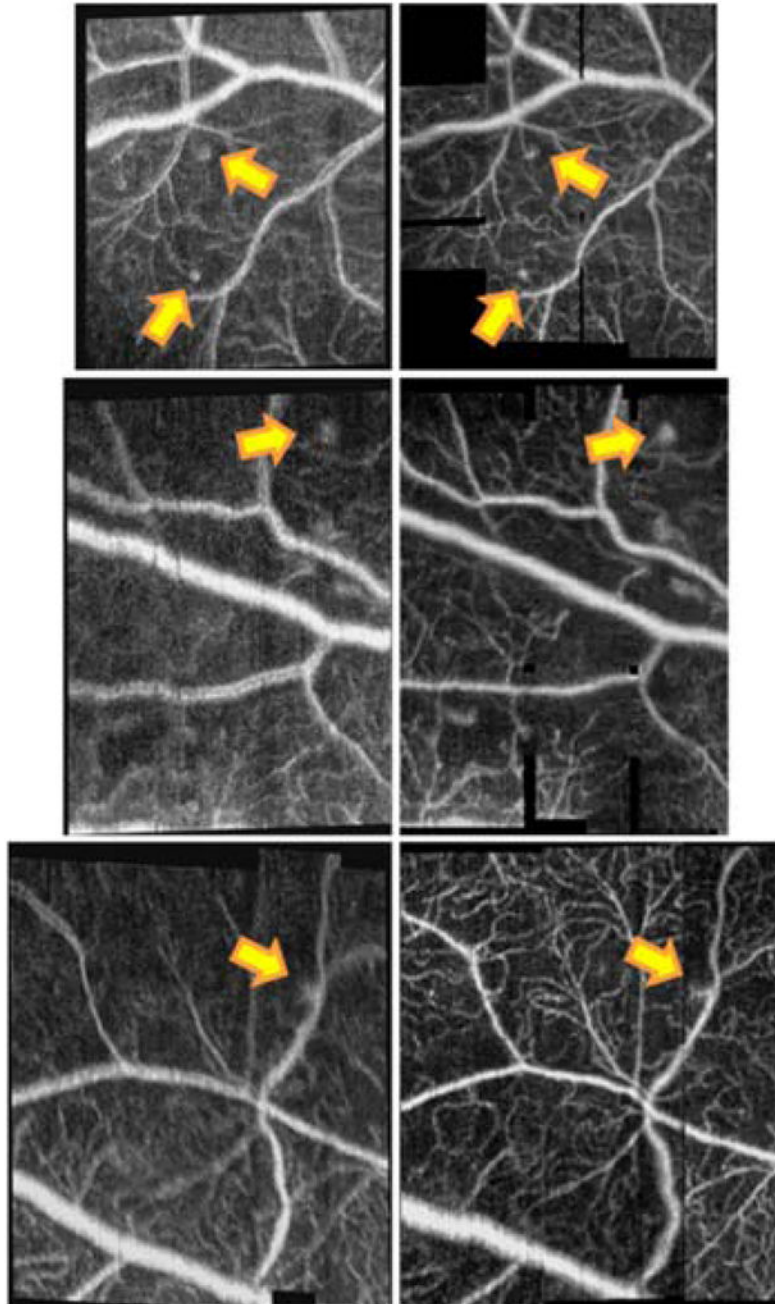
Fig. 3.
Targeted OCTA scans of peripheral microvasculature acquired without (left) and with (right) WSAO correction in volunteers with diabetic retinopathy. Note that the sites of peripheral microaneurysms (yellow arrows) improved with WSAO. The images are 1.66×1.92 mm (top, diabetic subject 1), 1.40×1.96 mm (middle, diabetic subject 1), 1.59×1.92 mm (bottom, diabetic subject 2) including the black space.
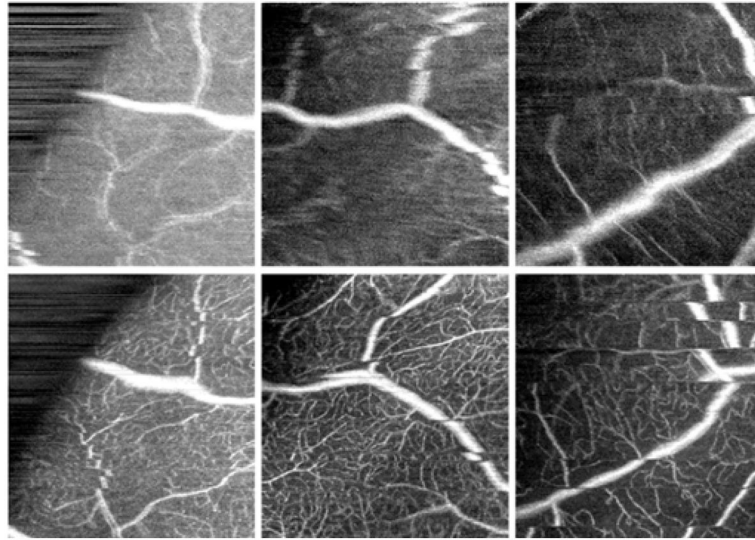
Fig. 4.
Targeted OCTA scans of peripheral microvasculature acquired without (top) and with (bottom) WSAO correction. The image pairs were not registered or motion corrected intentionally. These pairs highlight the improvement in image quality offered by WSAO even when motion correction is not available. All of the images are 1.87×2.00 mm. The left and middle images are from the healthy volunteer and the right images are from diabetic subject 3.